instruments

MDPI

Article

R&D of a Novel High Granularity Crystal Electromagnetic Calorimeter

Baohua Qi [1,2,3] and Yong Liu [1,2,3,*] on behalf of the CEPC Calorimeter Working Group

1 Institute of High Energy Physics, Chinese Academy of Sciences, Yuquan Road 19B, Beijing 100049, China
2 University of Chinese Academy of Sciences, Yuquan Road 19A, Beijing 100049, China
3 State Key Laboratory of Particle Detection and Electronics, Yuquan Road 19B, Beijing 100049, China
* Correspondence: liuyong@ihep.ac.cn; Tel.: +86-010-88236066

Abstract: Future electron-positron collider experiments aim at the precise measurement of the Higgs boson, electroweak physics and the top quark. Based on the particle-flow paradigm, a novel highly granular crystal electromagnetic calorimeter (ECAL) is proposed to address major challenges from jet reconstruction and to achieve the optimal EM energy resolution of around 2–3%/$\sqrt{E(\mathrm{GeV})}$ with the homogeneous structure. Extensive R&D efforts have been carried out to evaluate the requirements and potentials of the crystal calorimeter concept from sensitive detection units to a full sub-detector system. The requirements on crystal candidates, photon sensors as well as readout electronics are parameterized and quantified in Geant4 full simulation. Experiments including characterizations of crystals and silicon photomultipliers (SiPMs) are performed to validate and improve the simulation results. The physics performance of the crystal ECAL is been studied with the particle flow algorithm "ArborPFA" which is also being optimized. Furthermore, a small-scale detector module with a crystal matrix and SiPM arrays is under development for future beam tests to study the performance for EM showers.

Keywords: Higgs factory; calorimeter; crystal; SiPM; high granularity

check for updates

Citation: Qi, B.; Liu, Y., on behalf of the CEPC Calorimeter Working Group. R&D of a Novel High Granularity Crystal Electromagnetic Calorimeter. *Instruments* **2022**, *6*, 40. https://doi.org/10.3390/instruments6030040

Academic Editors: Fabrizio Salvatore, Alessandro Cerri, Antonella De Santo and Iacopo Vivarelli

Received: 31 July 2022
Accepted: 10 September 2022
Published: 15 September 2022

1. Introduction

The discovery of the Higgs boson in 2012 by the ATLAS [1] and CMS [2] Collaborations at the Large Hadron Collider (LHC) offers exciting opportunities for future particle physics in the coming decades. Precise measurements of properties of the Higgs boson, the W and Z bosons, as well as the top quark, will provide crucial tests of the standard model (SM) and are promising in searching for new physics beyond the SM (BSM). Following the demands from physics, future electron–positron colliders including the CEPC [3], FCC-ee [4], ILC [5] and CLIC [6] are among options planned to devote most of their operation hours as Higgs factories, to produce millions of Higgs bosons within a clean collision environment.

To fully exploit the physics potentials of a future lepton collider, the detectors should achieve an unprecedented jet energy resolution, which poses stringent requirements on the detector design. The invariant mass resolution of the Higgs boson aims to reach 3–4% at the CEPC. A jet is typically composed of ~65% charged particles, ~15% photons, and ~10% neutral hadrons. Particle flow algorithms [7] (PFA) aim to measure each of the final-state particles with one of the optimal sub-detectors and require high granularity in calorimeters to separate close-by particle showers and try to match with the tracking system for charged particles. A PFA-oriented electromagnetic calorimeter (ECAL) should be precise enough for photon energy reconstruction and particle identification (PID). Therefore, a highly segmented ECAL with excellent three-dimensional (3D) spatial resolution as well as good energy and time resolution is desired. Among the PFA-ECAL options that are being developed within the CALICE [8] Collaboration, e.g., the silicon-tungsten ECAL [9] and scintillator-tungsten ECAL [10], the energy resolution would be limited by the sampling structures (on the order of $\sim 10\%/\sqrt{E(\mathrm{GeV})}$). On the other hand, legendary crystal-based calorimeters have demonstrated excellent EM resolution of 2–3%/$\sqrt{E(\mathrm{GeV})}$ (for instance, the BGO calorimeter in the LEP-L3 experiment [11] and the PWO calorimeter in the LHC-CMS experiment [12]) while there was no fine 3D segmentation in crystals. Hereby, we propose a new conceptual design of the high granularity crystal ECAL with fine 3D segmentation to be compatible with the PFA, to reach an optimal EM resolution, and to significantly improve the sensitivity to low-energy particles. The precision measurements of γ and π^0 can also be portals to further explore the new physics beyond the standard model [13].

There are two major designs of the high granularity crystal ECAL in the proposal, as shown in Figure 1. Design 1, with finely segmented crystals in both longitudinal and transversal dimensions, would be naturally compatible with PFA. Initial PFA studies have been performed using this design to demonstrate the potentials in physics, which will be presented in Section 2. It also sets a stringent requirement on the total material budget of readout boards, cooling services and mechanical structures between longitudinal layers, which must be strictly controlled to avoid significant performance degradation [14].

To address this challenge, a new detector layout is proposed (Design 2 in Figure 1) with long crystal bars arranged to be orthogonal to each other in two neighboring layers for a maximum longitudinal segmentation, minimum inactive materials in between and a significant reduction in readout channels. High transverse granularity is expected to be realized by combining the information of every two adjacent layers. The basic module of a "supercell" is 40×40 cm^2 in the transverse plane with, typically, $24X_0$ in depth. Each crystal bar is read out by 2 SiPMs at two ends, which can also provide timing information from the two sides for positioning reconstruction, clustering and particle identification. Nevertheless, this layout also poses a challenge for 3D pattern recognition and requires the development of dedicated reconstruction software, which will be briefly introduced in Section 3.

Besides the highlights of physics performance studies and software development, preliminary results from hardware R&D activities on the key aspects of the calorimeter design are presented in Section 4, followed by the summary and prospects in Section 5. It should be noted that most results presented in this proceeding are selected from active working progress.

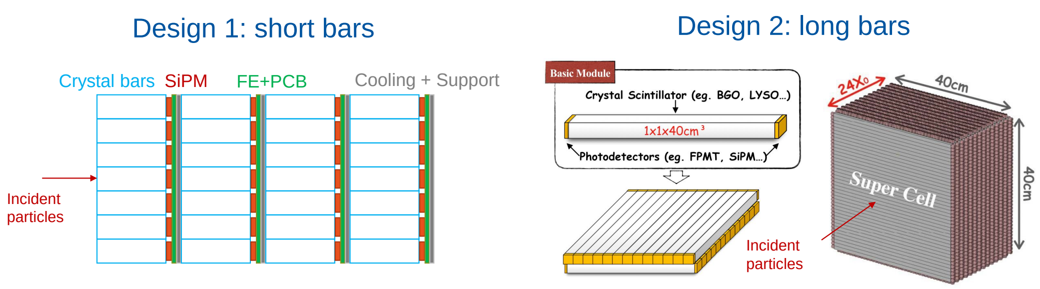

Figure 1. Two designs proposed for a high granularity crystal calorimeter: Design 1 with finely segmented crystals and single-ended readout; Design 2 with long crystal bars and two-ended readout.

2. PFA Performance

The CEPC baseline detector ("CEPCv4") in the CEPC Conceptual Design Report [3] and the PFA software "ArborPFA" [15] were implemented in the CEPC software framework [16] for the PFA performance studies and PFA optimizations. Baseline sub-systems from the inside out include silicon vertex detector, Time Projection Chamber (TPC), silicon-tungsten (SiW) ECAL, RPC-based HCAL, magnet coils and the return yoke as a muon detector, as shown in Figure 2a. The SiW-ECAL was replaced by finely segmented crystal bars with two sets of granularity, i.e., $1 \times 1 \times 1$ cm^3 and $1 \times 1 \times 2$ cm^3. The granularity of $1 \times 1 \times 1$ cm^3 corresponds to an ideal setup to fully exploit 3D information to evaluate the potentials and optimize the PFA parameters for crystals. The slightly coarser granularity of $1 \times 1 \times 2$ cm^3 is the goal for the layout of long crystal bars (Design 2), assuming that the dedicated reconstruction software can finally resolve ambiguities of pattern recognition in shower clustering due to the special geometry arrangement. The crystal option implemented for the crystal ECAL was selected to be the Bismuth Germanate (BGO) at this stage.

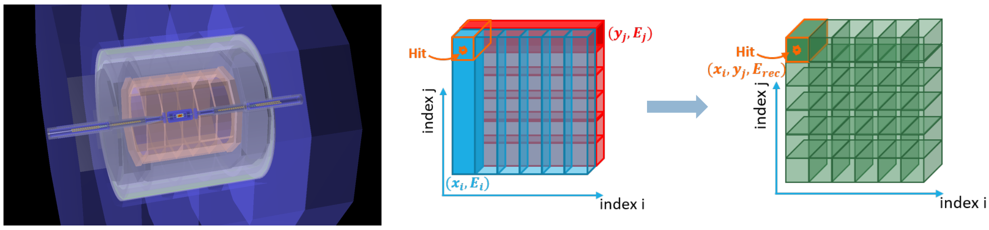

(**a**) (**b**)

Figure 2. The CEPC CDR detector layout ("CEPCv4") for PFA performance studies with implementations of the SiW-ECAL (as the CDR baseline) and crystal ECAL in two scenarios. (**a**) CEPC CDR baseline detector. (**b**) Reconstruction with long crystal bars with an aim of fine transverse granularity.

2.1. Separation Power of Close-By Showers

The separation capability of showers initiated by close-by particles is an essential requirement for PFA calorimetry. Considering typical jet components, key scenarios are: (1) the separation of two photons (denoted as $\gamma's$) and (2) the separation of a charged pion ($\pi^{\pm}$) and a γ [17].

Compared with the SiW-ECAL, EM showers in crystals tend to have a larger number of hits and a wider lateral distribution, since crystals are more sensitive to low-energy particles in secondary cascades and the Molière radius (R_M) for crystals ($R_M = 2.26$ cm for BGO) is significantly larger than tungsten ($R_M = 0.93$ cm) [18]. As the ArborPFA was optimized for the CEPC CDR with sampling calorimeters, it needs further optimizations to take into account different shower features in a homogeneous calorimeter.

Major updates implemented in the ArborPFA algorithm for the crystal ECAL include: (1) to search for the cluster skeleton using a relatively high energy threshold and by temporarily ignoring low-energy hits; and (2) to re-cluster low-energy hits near the shower skeleton. Simulation studies so far show that these two updates can significantly improve the separation capability (presented below) and energy linearity and resolution (not shown due to page constraints), respectively.

The separation of near-by particles is based on the overlay of events of single particles generated by a particle gun with varying positioning offsets. Showering events of γs and charged pions before entering the ECAL are excluded for further analysis. The separation efficiency is defined as the ratio of the events with two correctly reconstructed physics objects from ArborPFA algorithm (PFA Objects, or PFOs) and the total events. A correct reconstruction is defined as the PFO energy being in the range of 3.3–6.6 GeV for incident 5 GeV photons, and of 9.9–10.1 GeV for incident 10 GeV charged pions. The latter scenario corresponds to an essential part of the ArborPFA, i.e., cluster matching between trackers and calorimeters for charged particles, where trackers can provide the momentum information with much higher accuracy than calorimeters.

As shown in Figure 3, the separation efficiency of two $\gamma's$ increases along with a higher energy threshold (implemented for each crystal cell) in the updated ArborPFA with the multi-threshold reconstruction scheme. The performance of the granularity of $1 \times 1 \times 2$ cm^3 is similar to the ideal granularity of $1 \times 1 \times 1$ cm^3. It would be more challenging to separate hadronic clusters from EM ones, due to the complicated hadronic shower profiles leading to issues of matching the charged clusters in calorimeters with trackers. Clusters of the hadrons will be much more widely distributed in 3D space, and fluctuations in hadronic shower profiles and energy depositions are much more significant, compared with EM showers. Parameters concerning the distance between clusters and tracks can hardly be effective enough. For the particle-flow algorithms, there is always a significant chance that clusters originally from a hadron will not be correctly associated with its track.

It should be noted that the crystal ECAL geometry in simulation was kept the same as the SiW-ECAL layout, where gaps between modules are based on the SiW option. This study shows these gaps (e.g., around 160 mm in the plots) will degrade the separation efficiency of the crystal ECAL. A new general layout dedicated to crystal modules will be studied to include realistic estimates and minimize the impacts from gaps.

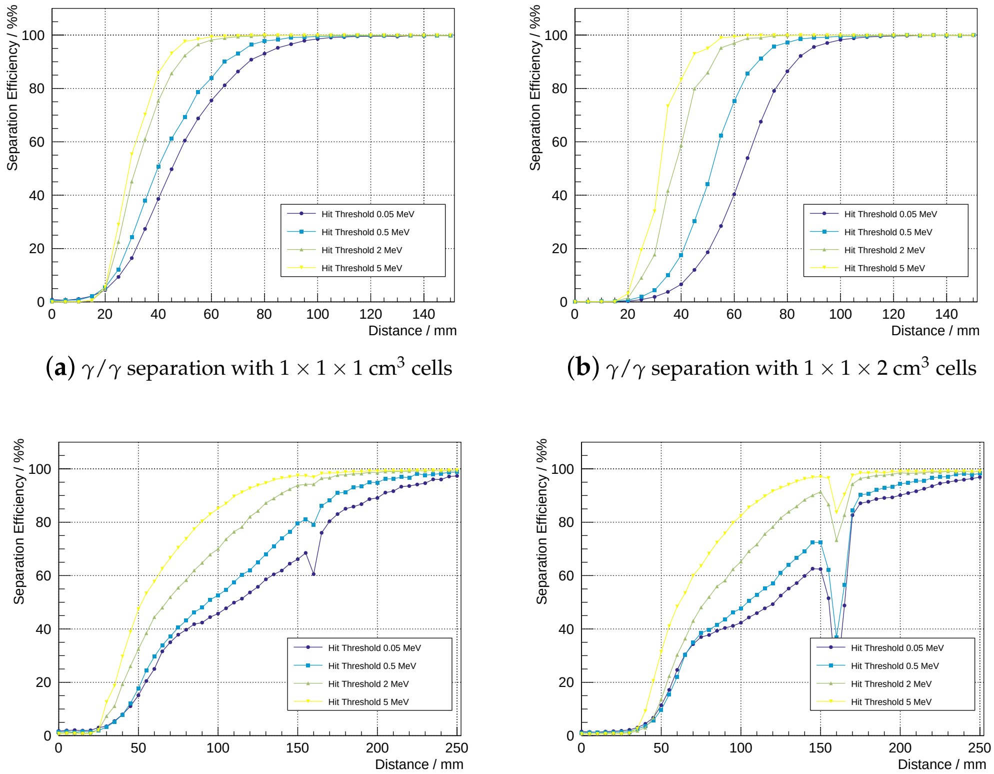

(**a**) γ/γ separation with $1 \times 1 \times 1$ cm^3 cells (**b**) γ/γ separation with $1 \times 1 \times 2$ cm^3 cells

(**c**) π^+/γ separation with $1 \times 1 \times 1$ cm^3 cells (**d**) π^+/γ separation with $1 \times 1 \times 2$ cm^3 cells

Figure 3. Separation efficiency with varying distances between two incident particles using two sets of crystal granularity.

2.2. Higgs Benchmark with Jets

The boson mass resolution (BMR) is a key parameter to evaluate the PFA performance of jets in Z/W/Higgs hadronic decays. At the CEPC, the Higgs BMR needs to be <4% in order to reach the 2σ separation power of the Higgs and Z/W bosons. The MC samples of $e^+e^- \rightarrow ZH \rightarrow \nu\nu gg$ including initial-state radiation (ISR) photons at 240 GeV were used for the studies with two gluon jets of the Higgs final state, where the BMR is defined as the invariant mass with two jets reconstructed by the ArborPFA. The simulation setup remains the same as in Section 2.1, i.e., the CEPC CDR baseline detector with the SiW-ECAL superseded by the crystal ECAL using the granularity of 1 cm^3. Since the default ArborPFA was optimized for the CEPC CDR baseline detector, as shown in Figure 4a, it cannot deliver the required performance with the crystal ECAL even with the fine granularity. After implementing the updates in ArborPFA as discussed in Section 2.1 for separation of close-by particles in crystals, there is a significant improvement in BMR by 3.7%, as shown in Figure 4b. Further optimizations and studies of impacts from granularity are ongoing.

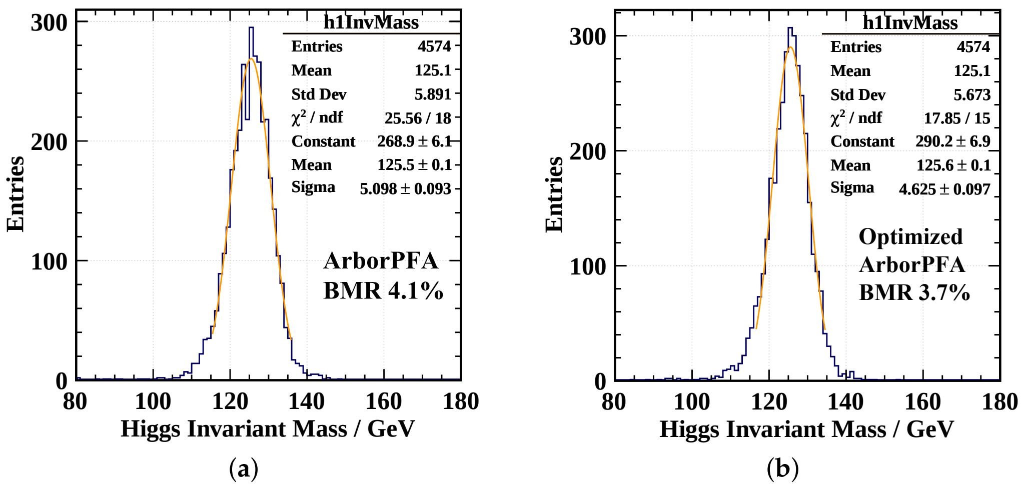

Figure 4. Higgs boson mass resolution with the ArborPFA algorithm. (**a**) BMR with the crystal ECAL using the default ArborPFA. (**b**) BMR with the crystal ECAL using the optimized ArborPFA.

3. Reconstruction Algorithm Dedicated to New Geometry Design

For the long bar layout, the geometry was implemented using DD4hep [19] and a dedicated reconstruction algorithm is under development in the new software framework named "CEPCSW" [20]. The idea is to start reconstruction from raw hits for each longitudinal layer to form 1D clusters and obtain 2D clusters by combining information from every two adjacent layers. Then, 2D clusters are linked in the longitudinal direction into 3D clusters required by the PFA. The basic reconstruction flow is shown in Figure 5. To reach its full physics potential, key questions including pattern recognition and cluster matching with the tracking system need to be addressed. In general, the new algorithm aims to achieve the granularity of $1 \times 1 \times 2\ \mathrm{cm}^3$, and minimize the impact from the ambiguity of pattern recognitions. In Figure 6, preliminary performance studies of the crystal ECAL with the long bar layout show promising results in particles reconstruction and separation [21]. Further development and validation works are still ongoing.

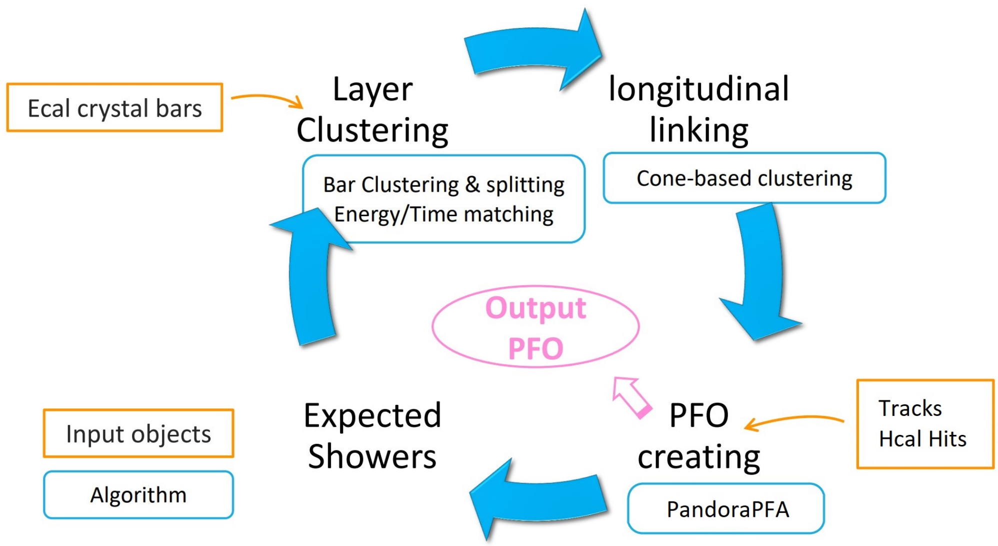

Figure 5. Dedicated reconstruction flow for the crossed long crystal bar ECAL.

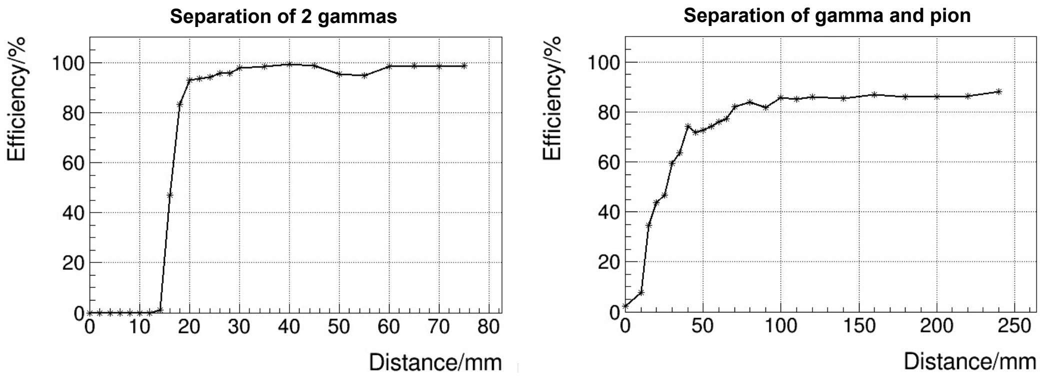

Figure 6. Preliminary study of separation efficiency with the dedicated reconstruction algorithm.

4. Detector Design and Characterizations

The quantitative requirements on the crystal and readout unit are presented in this section, including the EM energy resolution, photon statistics, energy threshold, and response uniformity, followed by measurements of a typical crystal-SiPM unit. Parameters in the digitization tool used by the Geant4 [22] simulation were tuned based on the cosmic-ray and radioactive test results.

4.1. Energy Resolution and Requirements

The EM energy resolution of the crystal calorimeter was studied with the Geant4 simulation (without the optical photon simulation). To take into account the important factors related to photon statistics, we developed a digitization tool to convert the raw energy deposition into the number of photons detected by a SiPM. The digitization tool includes the energy threshold per readout channel, fluctuations in photons detected at the SiPM, the time window for signal integration, etc. The photon statistics are primarily evaluated in terms of the MIP (minimum ionising particle) response, which corresponds to the most probable energy deposition of high energy muons in 1 cm BGO crystal around 8.9 MeV [18].

As shown in Figure 7a, the EM energy resolution for a given MIP response of 100 p.e. is dominated by the energy threshold per readout channel and the threshold should be lower than 0.5 MIP to achieve the aim of $<3\%/\sqrt{E(\mathrm{GeV})}$. The MIP light yield per channel, i.e., photo-statistics, significantly impacts the stochastic term extracted from the EM energy resolution, as shown in Figure 7b, and the MIP light yield is required to be more than 100 p.e. A sufficiently low energy threshold is always desirable to further improve the resolution. SiPMs with a low inter-pixel crosstalk level are promising to achieve a reasonably low energy threshold. For a good balance between the MIP light yield and the dynamic range, the appropriate crystal candidate needs to have a moderate intrinsic light yield. The crystal candidate is required to be friendly for mechanical processing (especially important for the long crystal bar design) and not prohibitively costly for the large volume usage required by the final detector (unit price on the order of a few USD per c.c.).

Crystal options under study primarily focus on the bismuth germanate (BGO). BGO has a high intrinsic light yield, in the range of 8000–10,000 photons/MeV, and its mechanical stability is good for cutting and polishing, but with a typical long scintillation decay time of 300 ns. The lead tungstate (PWO) has fast scintillation components (the fast and slow components are 10 ns and 30 ns, respectively), but its low intrinsic light yield, in the range of 100–200 photons/MeV, makes it difficult to meet the requirement of more than 100 p.e./MIP. Furthermore, it is quite brittle and, thus, further mechanical processing is very challenging, especially for long crystal bars.

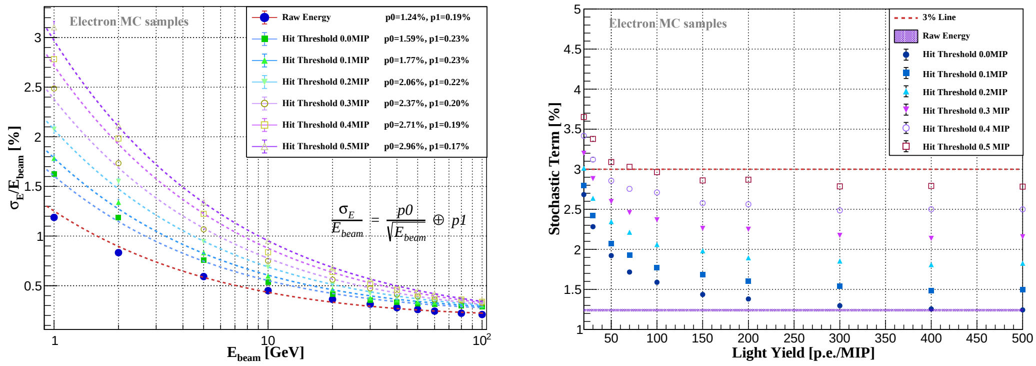

(**a**) (**b**)

Figure 7. Energy resolution under different energy thresholds and crystal light yields. (**a**) The EM energy resolution when different energy thresholds are implemented on calorimeter hits. The light yield is set to 100 detected photons per MIP. (**b**) The stochastic term of the EM energy resolution with varying light yields (number of detected photons per MIP) and energy thresholds for hits.

4.2. Laser Calibration of SiPMs

The SiPMs for the crystal ECAL readout need to cover a large dynamic range (on the order of 10^3 MIPs), which requires a high pixel density (on the order of 10^5 pixels for the total sensitive area). A laser test stand was built with a picosecond laser source (405 nm, NKT Photonics [23]) for SiPM characterizations including the single photon calibration and the response linearity. The SiPMs under test are listed in Table 1. In Figure 8, single photons can be well-separated for the two types of SiPMs, and the NDL-EQR06 SiPM is expected with better timing performance due to the fast-rising edge. The narrow pulse shape (~10 ns) is helpful to achieve an effectively larger dynamic range for crystals with a long decay time (e.g., BGO) due to the short recovery time of pixels. Results of ongoing measurements of the response linearity and the dynamic range will be presented in future conferences or papers.

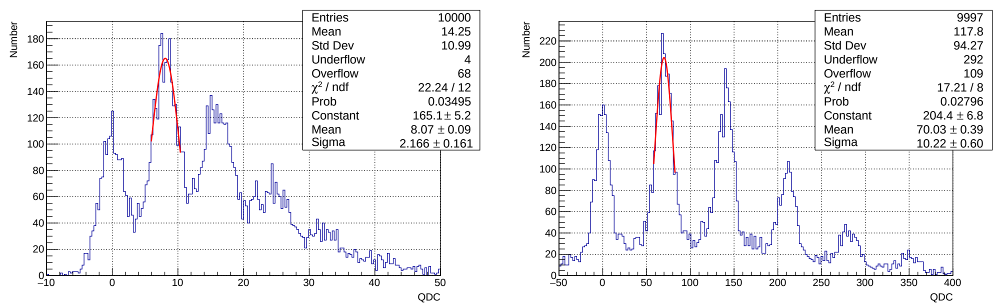

(**a**) Single photon spectrum of EQR06 SiPM (**b**) Single photon spectrum of S13360-6025PE SiPM

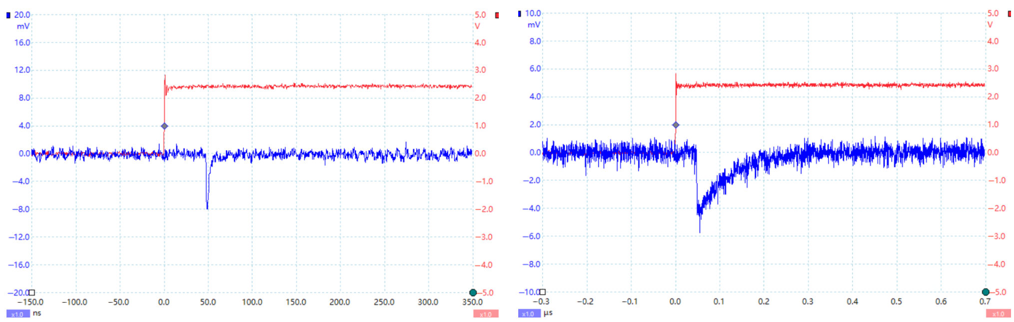

(**c**) The typical waveform of EQR06 SiPM (**d**) The typical waveform of S13360-6025PE SiPM

Figure 8. Single photon spectrum and typical waveforms in the oscilloscope of DUTs. Red pulses in (**c**,**d**) correspond to trigger signals.

Table 1. Devices under test and their basic parameters.

Type	Pixel Pitch (µm)	Sensitive Area (mm)	Number of Pixels	Typical PDE	Typical Gain
Hamamatsu S13360-6025PE [24]	25	6×6	57,600	25%	7×10^5
NDL EQR06 11-3030D-S [25]	6	3×3	244,720	30%	8×10^4

4.3. *Characterization of Long BGO Crystal Bar*

The characterizations of a 40 cm long BGO crystal bar (manufactured by the Shanghai Institute of Ceramics [26]) were carried out to evaluate the MIP response performance and the results are also used to validate the digitization tool.

4.3.1. Cosmic-Ray Test

A $1 \times 1 \times 40$ cm^3 BGO crystal was tested with cosmic-ray muons to evaluate the MIP response. As shown in Figure 9a, the crystal bar was wrapped with ESR film and placed onto a rail. Two apertures were cut out through the wrapping of the two ends for the light detection at SiPMs. Hamamatsu C13365-3050SA [27] SiPM modules (3×3 mm^2 active area) were coupled to the two sides of the crystal bar with silicone grease (index of refraction 1.465). In addition, two 3×3 cm^2 triggers were used to select coincidence muon events. The most probable value of the MIP response is 2028 p.e./MIP, as shown in Figure 9b. The fact that the trigger size is larger than the crystal cross section leads to a structure at the left side of the MIP signal, i.e., muons penetrates only partially but not the full crystal. It shows that the MIP response can meet the requirement, but we also need to consider the dynamic range as another critical issue, which remains under study.

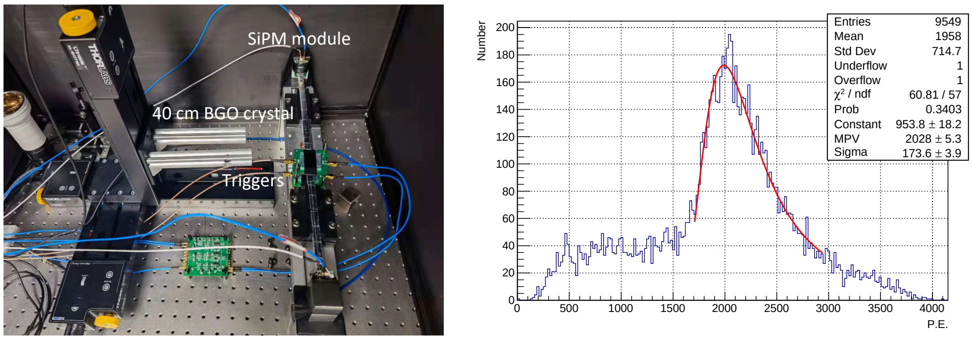

(**a**) A photo of the setup of the cosmic-ray test (**b**) Measured MIP response with BGO crystal

Figure 9. Setup and result of the cosmic-ray test of the BGO crystal.

4.3.2. Energy Calibration with a Radioactive Source

Measurements with radioactive sources are important to evaluate the energy resolution and to validate the digitization tool. Tests were performed with the same BGO crystal bar of $1 \times 1 \times 40$ cm^3 as mentioned above. Signals were read out by two SiPMs (Hamamatsu S13360-6025PE) directly air-coupled with each end. A slide rail system was used to improve the stability for better SiPM–crystal coupling. A radioactive source of Cs-137 was placed on the 1D movable rail to scan along the crystal length direction, as shown in Figure 10a. It should be noted that the source collimation diameter is around 8 mm. Figure 10b shows the energy resolution is 11.2% for 662 keV gammas, and the full-energy peak corresponds to around 134 p.e. at the SiPMs.

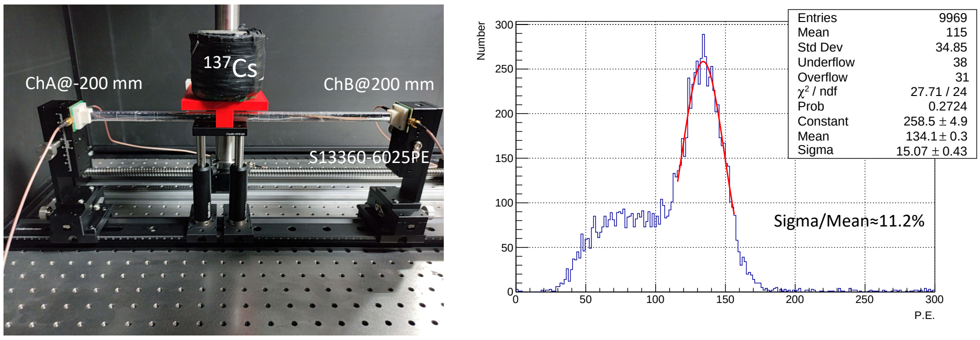

(**a**) A photo of the radioactive source test stand (**b**) Measured energy spectrum of Cs-137

Figure 10. Radioactive source test of a 40 cm long BGO crystal bar.

4.3.3. Response Uniformity Studies

The response uniformity along the crystal bar was measured with the same radioactive test-stand mentioned above by moving the radioactive source along the crystal bar length direction. The results from measurements and Geant4 optical simulation are shown in Figure 11a,b. The simulation assumed the intrinsic light yield of BGO crystals is 8200 p.e./MeV, and the crystal surface roughness was considered. Here, the incident-angle distribution of gamma-rays was not implemented and the simulation will be improved in the future.

Preliminary results show that the response uniformity in measurements is, in general, better than the simulation, but only features an asymmetrical pattern. In general, the results in data and simulation are reasonably consistent at a 10% level, which is sufficient for the validation of the optical simulation and the digitization tool at the first order. For better consistency of 1%, there are several subtle parts to be studied, such as optical model parameters and the modeling of defects on the crystal surface, guided by the measurements. On the other hand, more crystals will be tested to evaluate repetitive precision.

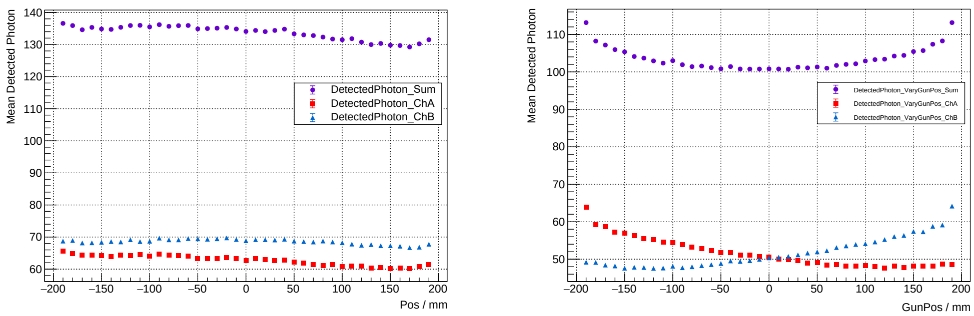

(**a**) (**b**)

Figure 11. Uniformity scan for a 40 cm long BGO crystal bar. (**a**) Measured response uniformity with Cs-137. (**b**) Simulated response uniformity with 662 keV photons.

A 2D uniformity map is obtained in simulation with muons perpendicularly passing through the module, as shown in Figure 12a, and was implemented in the digitization tool for an ECAL module with the transverse size of 40×40 cm^2 with the detector layout of crossed long crystal bars. The 2D non-uniformity effect will lead to position dependence for the energy reconstruction. Monte Carlo samples of high-energy electrons were used to evaluate the impacts on the energy reconstruction of EM showers, dependent on different levels of non-uniformity, as shown in Figure 12b. Therefore, the crystal-SiPM response uniformity needs to be well-controlled and carefully calibrated.

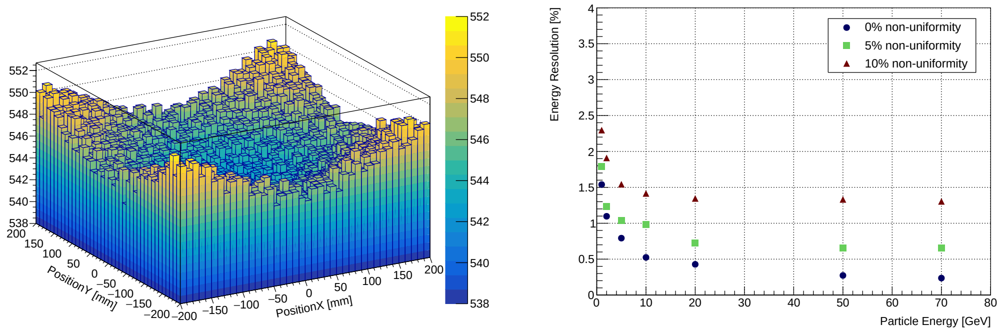

(**a**) (**b**)

Figure 12. Simulations of uniformity of the crystal ECAL module. (**a**) 2D response uniformity of the ECAL module, 1 GeV muons are used for scanning. (**b**) Energy resolution under certain non-uniformity of long crystal bars. Nine modules are placed in the simulation to prevent energy leakage.

5. Summary and Prospects

High-granularity calorimetry options enable an excellent jet reconstruction capability for future high-energy experiments. A highly granular crystal calorimeter was proposed to aim at a superior EM energy resolution and PFA performance for future Higgs factories. Physics potentials were presented using the CEPC detector with a high-granularity crystal calorimeter, including the PFA performance on separation power and the Higgs benchmark with two jets. The optimization of ArborPFA for crystals is ongoing. A dedicated reconstruction algorithm is under development for the detector layout with long crystal bars arranged to be orthogonal in adjacent layers. Hardware activities focus on the crystal–SiPM readout unit to address key questions of the detector requirements were studied. Characterizations of BGO crystals and SiPMs were carried out and the results were used to validate the simulation. In the near future, small-scale ECAL modules will be developed to evaluate the EM shower performance in beam tests, to gain experience in the large-scale module design, and to deliver reliable inputs to evaluate the whole detector performance.

Author Contributions: Conceptualization, Y.L.; methodology, B.Q. and Y.L.; software, B.Q.; validation, B.Q. and Y.L.; formal analysis, B.Q.; investigation, B.Q.; resources, Y.L.; data curation, B.Q. and Y.L.; writing—original draft preparation, B.Q.; writing—review and editing, Y.L.; visualization, B.Q.; supervision, Y.L.; project administration, Y.L.; funding acquisition, Y.L. All authors have read and agreed to the published version of the manuscript.

Funding: This project has received funding support from the Chinese Academy of Sciences (CAS) for young professionals and the CAS Center for Excellence in Particle Physics (CCEPP).

Data Availability Statement: The data presented in this study are available on request from the corresponding author. The data are not publicly available due to access restriction of the internal server.

Acknowledgments: The authors would like to express their gratitude for the fruitful discussions with many of the colleagues in the CEPC calorimeter working group and the CALICE collaboration.

Conflicts of Interest: The authors declare no conflict of interest.

References

1. The ATLAS Collaboration. Observation of a new particle in the search for the Standard Model Higgs boson with the ATLAS detector at the LHC. *Phys. Lett. B* **2012**, *716*, 1–29. [CrossRef]
2. The CMS Collaboration. Observation of a new boson at a mass of 125 GeV with the CMS experiment at the LHC. *Phys. Lett. B* **2012**, *716*, 30–61. [CrossRef]
3. The CEPC Study Group. CEPC Conceptual Design Report Volume II—Physics & Detector. *arXiv* **2018**, arXiv:1811.10545.
4. The FCC Collaboration. FCC-ee: The Lepton Collider - Future Circular Collider Conceptual Design Report Volume 2. *Eur. Phys. J. Spec. Top.* **2019**, *228*, 261–623. [CrossRef]
5. The ILC Collaboration. The International Linear Collider Technical Design Report Volume 4: Detectors. *arXiv* **2013**, arXiv:1306.6329.

6. Linssen, L.; Miyamoto, A.; Stanitzki, M.; Weerts, H. Physics and Detectors at CLIC: CLIC Conceptual Design Report. *arXiv* **2012**, arXiv:1202.5940.
7. Thomson, M.A. Particle flow calorimetry and the PandoraPFA algorithm. *Nucl. Instrum. Meth. A* **2009**, *611*, 25–40. [CrossRef]
8. CALICE Collaboration Home Page. Available online: https://twiki.cern.ch/twiki/bin/view/CALICE/WebHome (accessed on 20 July 2022).
9. The CALICE Collaboration. Design and electronics commissioning of the physics prototype of a Si-W electromagnetic calorimeter for the International Linear Collider. *J. Instrum.* **2008**, *3*, P08001.
10. The CALICE Collaboration. Construction and response of a highly granular scintillator-based electromagnetic calorimeter. *Nucl. Instrum. Meth. A* **2018**, *887*, 150–168. [CrossRef]
11. Adeva, B.; Aguilar-Benitez, M.; Akbari, H.; Alcaraz, J.; Aloisio, A.; Alvarez-Taviel, J.; Alverson, G.; Alviggi, M.G.; Anderhub, H.; Anderson, A.L.; et al. The construction of the L3 experiment. *Nucl. Instrum. Meth. A* **1990**, *289*, 35–102. [CrossRef]
12. The CMS Collaboration. The CMS Electromagnetic Calorimeter Project: Technical Design Report. 1997. Available online: https://cds.cern.ch/record/349375 (accessed on 20 July 2022).
13. Escrihuela, F.J.; Flores, L.J.; Miranda, O.G. Neutrino counting experiments and non-unitarity from LEP and future experiments. *Phys. Lett. B* **2020**, *802*, 135241. [CrossRef]
14. Liu, Y. High-Granularity Crystal Calorimeter: R&D Status. Online Mini-Workshop on a Detector Concept with a Crystal ECAL, 22–23 July 2020. Available online: https://indico.ihep.ac.cn/event/11938/contributions/14784/attachments/6980/7889/2020_0722_Crystal_ECAL_Status_YL.pdf (accessed on 21 August 2022).
15. Ruan, M.; Videau, H. Arbor, a new approach of the Particle Flow Algorithm. In Proceedings of the International Conference on Calorimetry for the High Energy Frontier, Paris, France, 22–25 April 2013.
16. CEPC Software Home Page. Available online: http://cepcsoft.ihep.ac.cn/ (accessed on 21 August 2022).
17. Yuexin, W. Crystal ECAL Design for CEPC. Online Mini-Workshop on a Detector Concept with a Crystal ECAL, 22–23 July 2020. Available online: https://indico.ihep.ac.cn/event/11938/contributions/14786/attachments/6967/7875/Yuexin_CrystalECALWS_20200722.pdf (accessed on 21 August 2022).
18. PDG: Atomic and Nuclear Properties of Materials (2022). Available online: https://pdg.lbl.gov/2022/AtomicNuclearProperties/index.html (accessed on 21 August 2022).
19. DD4hep (Detector Description for High Energy Physics). Available online: https://github.com/AIDASoft/DD4hep (accessed on 20 July 2022).
20. CEPCSW (CEPC Offline Software Prototype Based on Key4hep). Available online: https://github.com/cepc/CEPCSW (accessed on 20 July 2022).
21. Fangyi, G. High-granularity Crystal ECAL for CEPC. The 2021 International Workshop on the High Energy Circular Electron Positron Collider, 8–12 November 2021. Available online: https://indico.ihep.ac.cn/event/14938/contributions/35587/attachments/17472/19907/CrystalECAL_CEPCWorkshop2021.pdf (accessed on 21 August 2022).
22. The GEANT4 Collaboration. Geant4—A simulation toolkit. *Nucl. Instrum. Meth. A* **2003**, *506*, 250–303. [CrossRef]
23. NKT PILAS—Picosecond Pulsed Diode Lasers Datasheet. Available online: https://www.nktphotonics.com/products/pulsed-diode-lasers/pilas/ (accessed on 20 July 2022).
24. Hamamatsu Photonics S13360 Series MPPC Datasheet. Available online: https://www.hamamatsu.com/content/dam/hamamatsu-photonics/sites/documents/99_SALES_LIBRARY/ssd/s13360_series_kapd1052e.pdf (accessed on 20 July 2022).
25. NDL (Novel Device Laboratory) EQR06 11-3030D-S SiPM Datasheet. Available online: http://www.ndl-sipm.net/PDF/Datasheet-EQR06.pdf (accessed on 20 July 2022).
26. Shanghai Institute of Ceramics, Chinese Academy of Sciences Home Page. Available online: http://english.sic.cas.cn/ (accessed on 20 July 2022).
27. Hamamatsu Photonics C13365 Series MPPC Module Datasheet. Available online: https://www.hamamatsu.com/content/dam/hamamatsu-photonics/sites/documents/99_SALES_LIBRARY/ssd/c13365_series_kacc1227e.pdf (accessed on 21 August 2022).